

Thermal stability of advanced Ni-base superalloys

H. M. TAWANCY, N. M. ABBAS, A. I. AL-MANA

Metrology, Standards and Materials Division, Research Institute, King Fahd University of Petroleum and Minerals, PO Box 1639, Dhahran 31261, Saudi Arabia

T. N. RHYS-JONES

Turbine Aerofoils Research and Development and Surface Technology, Rolls-Royce plc, PO Box 31, Derby DE24 8BJ, UK

Exposures consisting of 1 to 900 h at 1000 and 1100 °C after an ageing treatment of 16 h at 870 °C were used to study the thermal stability of selected γ' -strengthened Ni-based superalloys representing conventional, directional solidification, and single-crystal castings. Various techniques of microscopy, spectroscopy and diffraction were used to characterize the microstructure. Primary MC carbides in the alloys studied were found to be stable toward decomposition into lower carbides. In the aged condition, the strengthening γ' phase assumed a cuboidal morphology; however, all alloys also contained varying proportions of coarse lamellar γ' and hyperfine cooling γ' . On an atomic scale, the nature of the cuboidal γ' -matrix interface was found to vary from coherent to partially coherent. However, the overall lattice mismatch varied from one alloy to another depending upon its composition and the distribution of various elements in carbide phases and lamellar γ' phase. Directional growth of the cuboidal γ' phase upon exposure to higher temperatures was found to be accelerated by a large initial lattice mismatch leading to a considerable loss of coherency, as indicated by the observation of dislocation networks around the γ' particles. Although the composition of the γ' phase remained essentially unchanged, there was a marked change in matrix composition. Sigma phase was found to precipitate in all alloys, but its thermal stability was a function of alloy composition. The initial decrease in hardness followed by a hardening effect during exposure could be explained in terms of the partial dissolution of the γ' phase and precipitation of sigma phase.

1. Introduction

Although structural applications of ceramics, composites and intermetallics in gas turbine engines may have potential for extending their temperature capabilities [1], it is unlikely that these materials could replace the superalloys at least in the foreseeable future [2]. Improvements in engine thrust, fuel consumption and durability continue to be largely dependent upon advances in superalloy technology as well as cooling systems. Advances in casting-alloy development as well as the improvement in melting practices have significantly contributed to increasing the temperature capabilities of Ni-base superalloys strengthened by the γ' phase [3–6]. Directional solidification [7, 8] and single-crystal castings [8] are among the most important techniques developed to control the microstructure. In most advanced superalloys, the strength of the γ' phase is optimized by additions of Ti and Ta, and additional strengthening of the matrix solid solution (γ phase) is provided by additions of Mo, W and Re [9, 10].

Extensive reviews have dealt with the mechanical properties of the γ' phase based upon the Ni₃Al composition as well as γ' -containing alloys [11, 12]. Typically, the mechanical properties of γ' -strengthened alloys are evaluated after solution annealing, and a standard ageing treatment designed to precipitate the strengthening γ' phase. Subsequent prolonged exposure to higher temperatures, however, can cause significant changes in the volume fraction and morphology of the γ' phase [13–19]. Misfit dislocations between the γ' and γ phases can form readily either during prolonged exposure to elevated temperatures [13] or during plastic deformation [20, 21], resulting in loss of coherency between the two phases. Other important microstructural changes include precipitation of topologically close-packed phases such as the sigma phase [20, 21] and decomposition of primary carbides [19, 22, 23].

It was the objective of this investigation to study the thermal stability of selected Ni-base superalloys representing three classes of castings: (i) conventional

(Inconel alloy IN 100), (ii) directional solidification (alloy MAR M 002 DS), and (iii) single crystal (alloys RR 2000 and SRR 99)*.

2. Experimental procedure

Table I summarizes the nominal chemical compositions of the alloys investigated. As can be seen, alloy RR 2000 is essentially the single-crystal version of the cast alloy IN 100 where grain-boundary strengthening elements such as C, B and Zr are eliminated. Similarly, alloy SRR 99 is the single-crystal version of alloy MAR M 002 DS.

Specimens examined were in the form of rods about 20 mm in length and 8 mm in diameter. All specimens were heat-treated for 1 h at 1100 °C in argon atmosphere, air-cooled, aged for 16 h at 870 °C in argon and finally cooled in argon. Henceforth, this will be referred to as the aged condition. The mean blade temperature during engine operation is usually about 900–1000 °C, but the temperature may locally rise to 1100 °C due to hot-spot conditions. To cover this range, aged specimens were exposed for 1, 8, 24, 100, 500 and 900 h at 1000 and 1100 °C to study the thermal stability of each alloy.

Light optical metallography, scanning electron microscopy (SEM) and the transmission electron microscopy (TEM) mode of an analytical electron microscope (AEM) were used to characterize the microstructure. Structural analysis was conducted by X-ray diffraction using CuK_α radiation. Energy- and wavelength-dispersive X-ray spectroscopy (EDXS and WDXS, respectively) were used to determine the microchemical composition of bulk specimens in the SEM. Also, EDXS employing an ultra-thin window detector was used to determine the microchemical composition of thin-foil specimens in the scanning transmission electron microscopy (STEM) mode of an AEM.

TABLE I Nominal chemical compositions of the alloys studied

Element	Composition (wt%)			
	IN 100	RR 2000	MAR M 002 DS	SRR 99
Cr	9.5	10	9	8.5
Al	5.5	5.5	5.5	5.5
Ti	4.75	4	1.5	2.2
Co	15	15	10	5
Mo	3	3	0.5 ^a	0.5 ^a
W	0.2 ^a	0.5 ^a	10	9.5
Ta	—	0.05 ^a	2.5	2.8
Hf	—	0.05 ^a	1.25	0.05 ^a
V	0.95	1	—	—
Zr	0.95	0.01 ^a	0.055	0.01 ^a
Fe	1 ^a	0.1 ^a	0.5 ^a	0.1 ^a
B	0.015	—	0.015	—
C	0.175	0.015	0.15	0.015
Ni	Bal.	Bal.	Bal.	Bal.

^a Maximum.

* Inconel is a registered trademark of the Inco family of companies, MAR M is a registered trademark of Martin Marietta Corporation, while SRR and RR are registered trademarks of Rolls-Royce plc.

Specimens for light optical metallography were etched in Marble's reagent (10 g copper sulphate, 50 ml HCl and 50 ml H₂O). As-polished specimens were used for structural analysis by X-ray diffraction. Thin-foil specimens for AEM experiments were prepared by the jet polishing technique in a solution consisting of 30% nitric acid in methanol at about – 20 °C. All specimens were examined at 200 kV.

3. Results and discussion

3.1. Microstructure in the aged condition

Fig. 1 illustrates light optical micrographs and X-ray diffraction patterns derived from the alloys studied in the aged condition. Occasionally, voids typical of cast metal products were observed, particularly in the single-crystal alloys. All alloys contained MC carbides assuming script, cubic and/or semi-rounded morphologies. However, the cubic morphology was particularly pronounced in alloy MAR M 002 which could be related to the presence of Hf [24]. As expected, the polycrystalline alloys (IN 100 and MAR M 002) contained greater densities of MC carbides in comparison with their single-crystal versions (RR 2000 and SRR 99).

In addition to reflections of the matrix (γ phase, face-centred cubic solid solution), all diffraction patterns contained characteristic superlattice reflections of the γ' phase ($L1_2$ superlattice, face-centred cubic) such as the (100) and (110) as shown in Fig. 1. Since the volume fraction of carbide phases in each alloy was less than about 10%, no carbide reflections were observed. As shown in Fig. 1a, alloy IN 100 had a random grain orientation; however, because of the relatively small diameter of the X-ray beam in comparison with grain size, the intensities of some reflections were unusually high. For the directionally solidified alloy MAR M 002 and the single-crystal alloys RR 2000 and SRR 99, the (200) reflections were the most intense, reflecting the normal $\langle 100 \rangle$ growth direction [25].

For all alloys studied, the γ' phase assumed three distinct morphologies: (i) lamellar, (ii) cuboidal and (iii) spherical, but the cuboidal morphology was predominant. Coarse lamellar γ' was particularly observed near the surface as shown in Fig. 2. Evidently, this form of γ' had formed during solidification and could not be completely redissolved during solution annealing [25]. Because of the 75–100 °C higher melting range of the single-crystal alloys in comparison with the polycrystalline versions, they contained greater proportions of lamellar γ' .

Fig. 3 illustrates the cuboidal γ' phase providing the main source of mechanical strength and which had formed during thermal ageing. All alloys studied contained about the same volume fraction of cuboidal γ' (68–70%), estimated metallographically using the point counting method [26]. The average particle size ranged from about 0.32 μm in alloy SRR 99 to 0.63 μm in alloy IN 100. Such a range of particle size is

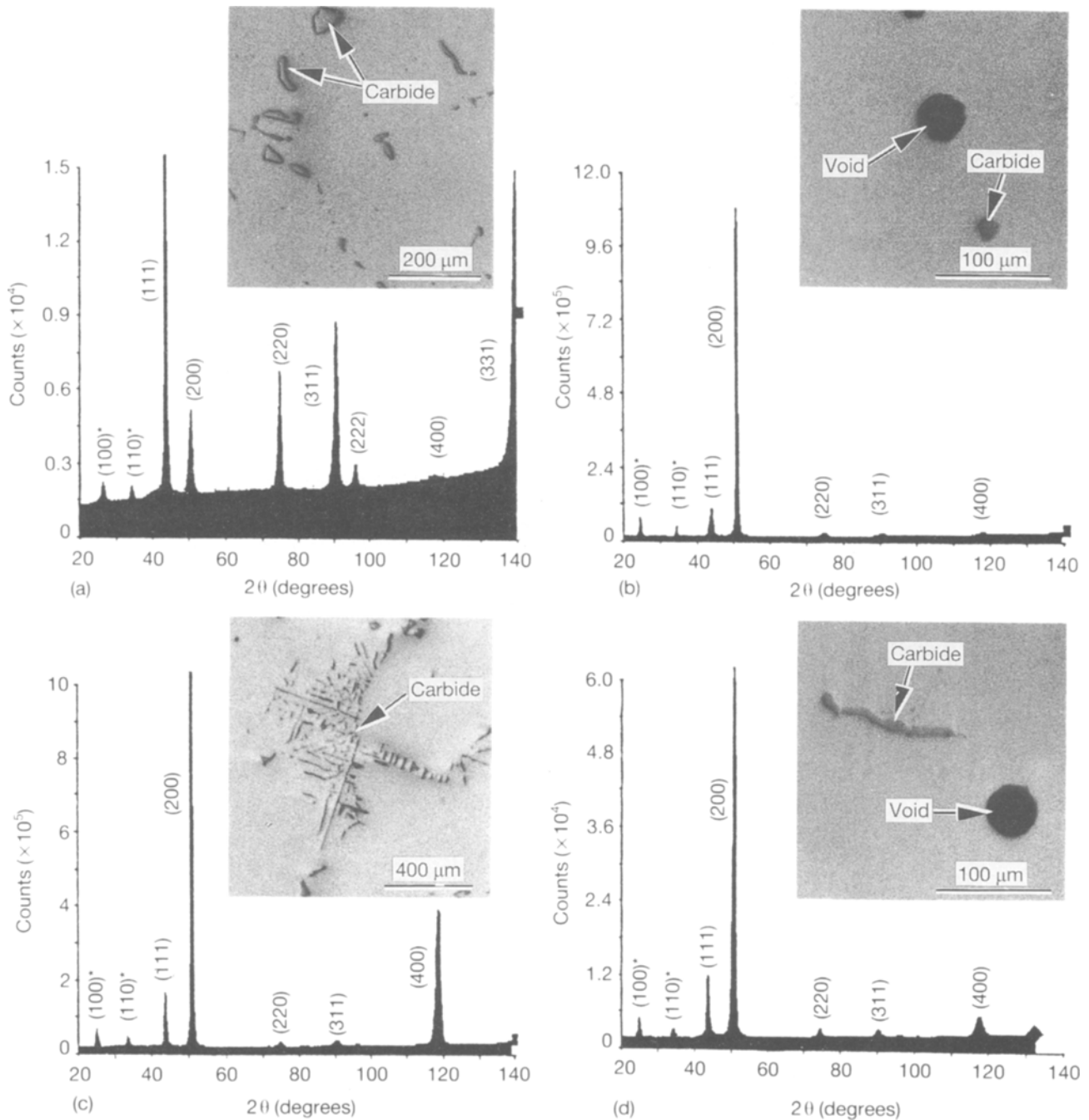


Figure 1 Light optical micrographs (as-polished specimens) and X-ray diffraction patterns derived from the alloys studied in the aged condition: (a) IN 100, (b) RR 2000, (c) MAR M 002 DS, (d) SRR 99. Asterisks indicate $L1_2$ superlattice reflections.

typically used to compromise between strength and ductility [27].

Previous work had demonstrated that the volume fraction of γ' phase formed in an alloy after a given ageing treatment is only a function of the atomic concentrations of γ' -forming elements, particularly Al, Ti, Ta and Hf [6, 22, 23, 29]. However, the (Al + Ti) concentration is considered the most significant in determining the volume fraction of γ' phase [6]. It was shown that increasing the (Al + Ti) concentration above the level characteristic of alloy IN 100 had no significant effect on the volume fraction of γ' phase because insignificant amounts of these elements above that level could be precipitated in the form of γ' phase [6]. As shown in Table I, all the alloys studied contained the same Al concentration. Although alloys

MAR M 002 and SRR 99 contained less Ti in comparison with alloys IN 100 and RR 2000, all alloys contained about the same volume fraction of γ' phase as summarized in Table II, suggesting that the presence of both Ta and Hf in alloy MAR M 002, and Ta in alloy SRR 99, could have compensated for the reduced Ti content. Based upon analysis of extraction residues, it has also been suggested that W could increase the volume fraction of γ' phase [15]. However, as shown later, only the lamellar γ' which is unavailable for strengthening [25] was found to be enriched in W (alloys MAR M 002 and SRR 99) and the strengthening cuboidal γ' was relatively free of W.

Some investigations of the growth kinetics of γ' have suggested that at a given ageing temperature, the particle size increases with the (Al + Ti) content of the

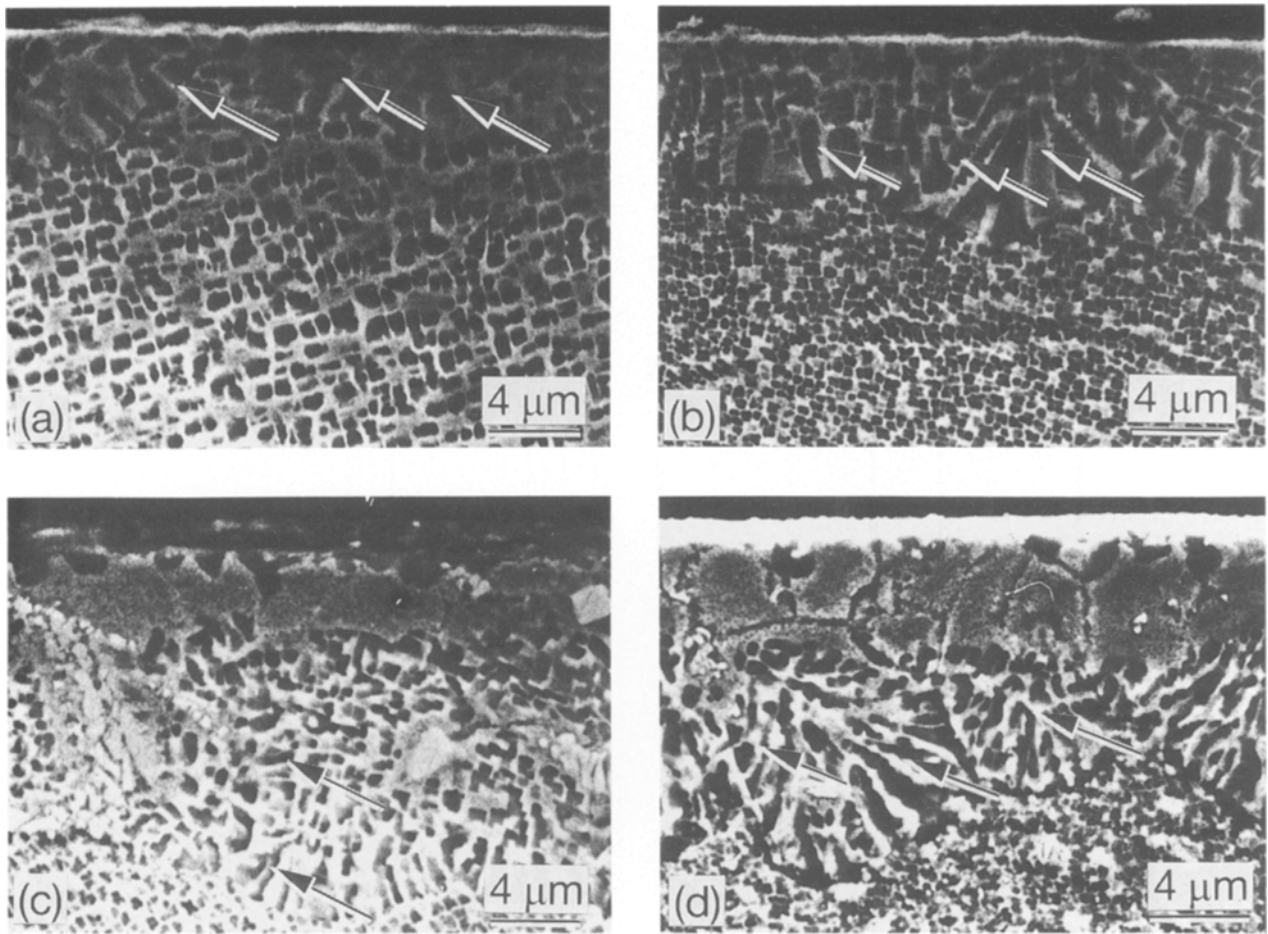


Figure 2 Secondary electron SEM images of alloys illustrating lamellar γ' near the surface as indicated by the arrows (aged condition): (a) IN 100, (b) RR 2000, (c) MAR M 002 DS, (d) SRR 99.

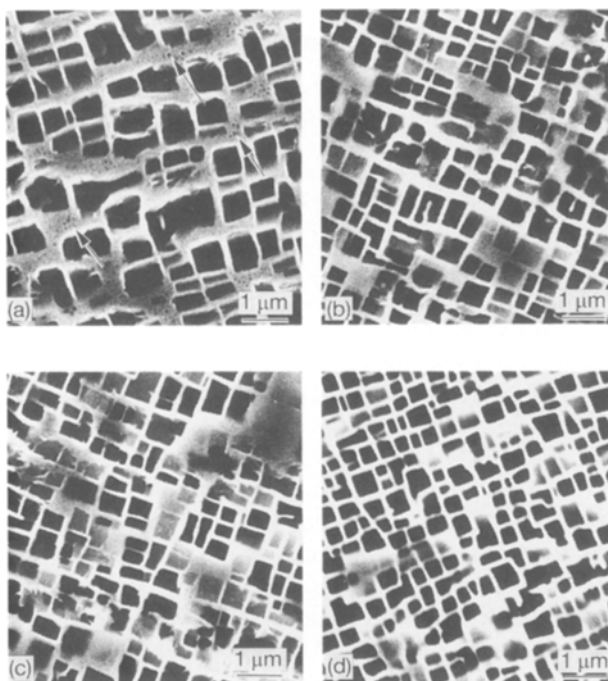


Figure 3 Secondary electron SEM images illustrating cuboidal γ' phase in the alloys studied (aged condition): (a) IN 100, (b) RR 2000, (c) MAR M 002 DS, (d) SRR 99.

TABLE II Effect of alloy composition on volume fraction of γ' phase

Alloy	Al + Ti + Ta + Hf content (at %)	Volume fraction of cuboidal γ' (%)
IN 100	16.42	68
RR 2000	15.73	70
MAR M 002 DS	15.16	68
SRR 99	15.61	68

alloy [30, 31]. However, it was also argued that the particle size is only a function of ageing temperature and time [29]. Although the possible dependence of particle size on the (Al + Ti) content appeared to be valid in the case of alloys IN 100 and RR 2000, it could not explain the observed difference between alloys MAR M 002 and SRR 99. Also, a dependence on ageing temperature and time only could not explain the observed differences in Fig. 4, since all alloys were given the same ageing treatment. However, as described below, differences in Co content could be a contributing factor.

Cobalt has long been known to significantly influence the γ' solvus temperature, depending upon the

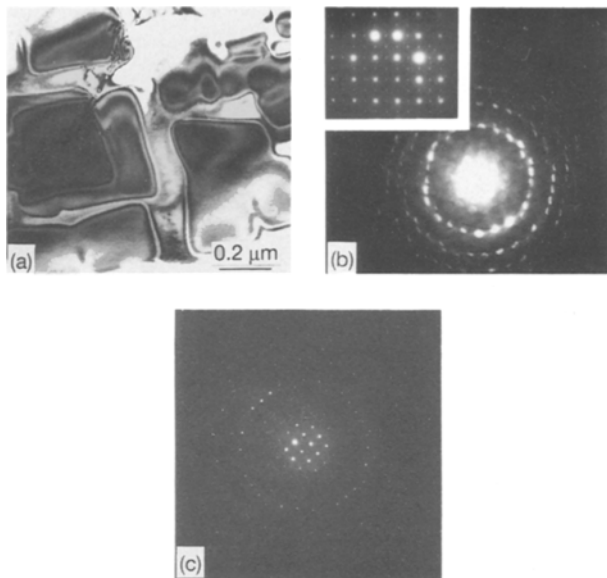


Figure 4 An example illustrating convergent-beam electron diffraction analysis to determine the lattice constants of the γ' and γ phases in alloy IN 100: (a) Bright-field TEM image illustrating cuboidal γ' particles. (b) $[001]$ convergent-beam diffraction pattern representative of the γ' phase; the zero-order Laue zone is shown in the inset where characteristic reflections of the $L1_2$ superlattice of γ' phase are observed at $\{100\}$, $\{110\}$ and all equivalent positions. (c) $[001]$ convergent-beam diffraction pattern representative of the γ phase (matrix solid solution).

relative concentrations of Al and Ti [28, 32, 33]. If the Ti content of the alloy is greater than that of Al, reducing the Co content has the effect of lowering the γ' solvus temperature [32]. In contrast, if the Al content is greater than that of Ti as in the present study (Table I), reducing the Co content has the effect of raising the γ' solvus temperature [28, 33]. Therefore, the γ' solvus temperature of alloy SRR 99 (5% Co) would be expected to be higher than that of alloy MAR M 002 (10% Co). At a given ageing temperature, the degree of undercooling of alloy SRR would be greater in comparison with alloy MAR M 002, leading to a greater nucleation site frequency and finer particle size as observed.

Only in the case of alloy IN 100, the spherical γ' which had formed during cooling from the ageing temperature could be resolved on the scale of SEM as indicated by the arrows in Fig. 3a. As can be seen, the cooling γ' formed in between the cuboidal γ' particles. For the other alloys, the cooling γ' could only be resolved on the scale of TEM. Variations in particle size from one alloy to another followed the same pattern as the cuboidal γ' .

Convergent-beam diffraction analysis such as that shown in the example of Fig. 4 as well as X-ray diffraction data (Fig. 1) indicated that the *in situ* lattice constant of the cuboidal γ' in all alloys studied was greater than the lattice constant of the respective matrix phase. Table III summarizes the lattice mismatch for each alloy. As can be seen, the lattice mismatch for all alloys was greater than 0.5% and less than 1%, which is consistent with the observed cuboidal morphology [22, 24]. Since W would be expected to expand the matrix lattice, its presence in relatively

TABLE III Comparative lattice mismatch between cuboidal γ' phase and matrix phase (γ)

Alloy	Lattice mismatch, ^a $\delta = (a_{\gamma'} - a_{\gamma})/a_{\gamma}$
IN 100	0.65
RR 2000	0.79
MAR M 002 DS	0.55
SRR 99	0.59

^a a = lattice constant.

large concentrations in alloys MAR M 002 and SRR 99 (Table I) could explain their comparatively smaller lattice mismatch. However, the lattice mismatch of alloy SRR 99 was slightly greater than that of alloy MAR M 002, probably because of the higher Ti content of alloy SRR 99. In contrast, alloy RR 2000 exhibited a considerably greater lattice mismatch in comparison with alloy IN 100. Other than alloy composition, distribution of various elements such as Mo, W, Ti and Ta in lamellar γ' phase and carbide phases could significantly influence the lattice mismatch, as described in the next sections.

An example illustrating the extent of coherency between the γ' and γ phases of alloy RR 2000 is given in Fig. 5. As expected, the γ' phase maintained a cube-to-cube orientation relationship with the γ phase as illustrated in the dark-field TEM experiment of Fig. 5a–c. It is well known that both coherent and partially coherent particles maintain a crystallographic orientation relationship with the surrounding matrix phase [34]. Trace analysis by selected-area diffraction (Fig. 5a–c) as well as by electron-channelling diffraction (Fig. 5d and e) revealed that the γ' particles were not perfectly aligned along $\langle 001 \rangle$ directions. It is evident from Fig. 5d and e, where the normal to the specimen surface was exactly $\langle 001 \rangle$ as determined from electron-channelling diffraction (Fig. 5d), that the γ' - γ interface locally deviated from $\{001\}$ planes. A further confirmation was provided by high-resolution lattice imaging of the interface (Fig. 5f) where misfit dislocations of edge character were observed about every ten atomic spacings, suggesting that the nature of the interface varied from perfect coherency to partial coherency. Similar results were obtained for the other alloys studied, but the extent of deviation from perfect coherency varied according to the respective lattice mismatch (Table III). As demonstrated later, this variation was reflected by the growth kinetics during exposure at higher temperatures.

3.2. Thermal stability of carbide phases

Although in many superalloys, MC carbides formed during solidification tend to decompose into lower carbides such as $M_{23}C_6$ during ageing treatment at lower temperatures [22], there was no evidence for carbide reactions in any of the alloys studied. In both the solution-annealed and aged conditions as well as after up to 900 h of exposure at 1000 and 1100 °C, the compositions and lattice parameters of all carbides

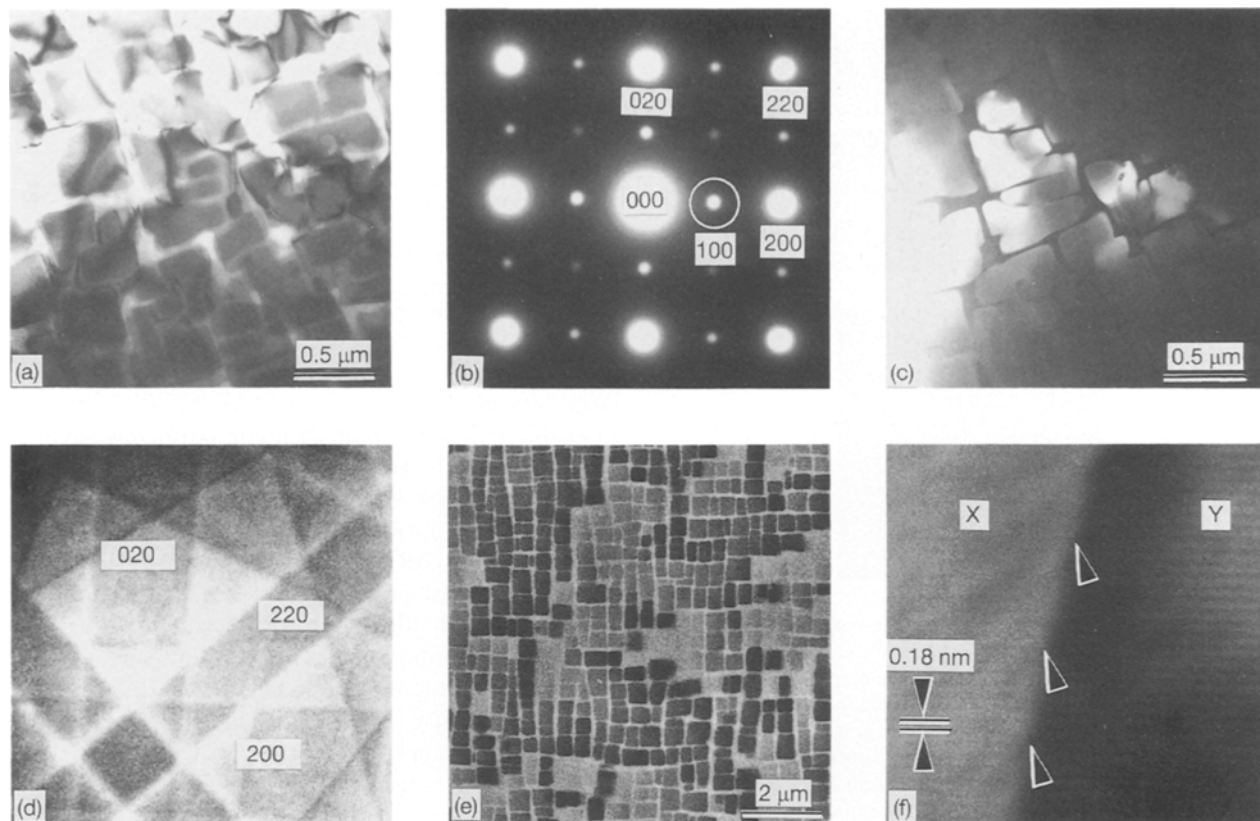


Figure 5 An example illustrating the extent of coherency between the γ' and γ phases of alloy RR 2000 in the aged condition. (a) Bright-field TEM image illustrating cuboidal γ' phase. (b) Corresponding $[001]$ selected-area diffraction pattern; characteristic reflections of the $L1_2$ superlattice of the γ' phase are observed at $\{100\}$, $\{110\}$ and all equivalent positions. (c) Dark-field image formed with the encircled (100) superlattice reflection in (b). (d) $[001]$ electron channelling diffraction pattern derived from the specimen surface. (e) Secondary electron SEM image corresponding to the pattern in (d). (f) One-dimensional lattice fringe image of (100) planes; fringe displacement at the γ - γ' interface is indicated by the arrows.

were essentially identical. Therefore, the examples given below are representative of the above conditions.

Only one type of MC carbide could be detected in alloy IN 100 and its single-crystal version alloy RR 2000. Analysis by TEM-STEM suggested that this carbide was of the type $(Ti_{0.8}Mo_{0.2})C$ with trace amounts of Ni, Co and Cr (cubic; $a = 0.419$ nm) as illustrated in the example of Fig. 6. Such a type of MC carbide was reported to be present in alloy Rene'77 [22].

In the case of alloy MAR M 002, two types of MC carbides were identified. As illustrated in the conventional SEM-EDXS analysis of Fig. 7, one type of carbide was enriched in Ta and Ti, i.e. of the type $(Ta,Ti)C$, and the other was Hf-rich, i.e. of the type HfC. Both carbides contained trace amounts of Ni and Cr. Fig. 8 illustrates an example of analysing the Ta- and Ti-rich carbide by TEM-STEM (cubic; $a = 0.448$ nm). A similar analysis indicated that the lattice parameter of HfC (cubic) was 0.461 nm. Only a carbide of the type $(Ta,Ti)C$ was observed in alloy SRR 99 which is free of Hf (Table I).

Examples illustrating the effect of up to 900 h of exposure at 1000 and 1100 °C on the composition of various carbide phases in the alloys studied are summarized in Fig. 9. As can be seen, the composition of

each carbide remained essentially unchanged. The presence of Ta has been reported to stabilize MC carbides toward chemical decomposition at lower temperatures, i.e. during ageing [24]. It is also evident from the above results that other refractory elements such as Hf and Mo could behave in a manner similar to that of Ta.

In relation to the γ - γ' lattice mismatch, elements present in carbide phases which could partition to the Al sublattice in the γ' phase such as Ta and Ti were suggested to have no significant effect on the lattice parameter of the γ phase; however, elements such as Mo and W which partition to the γ phase could have a significant effect [28]. Both Ta and Ti, however, were shown to increase the lattice parameter of the γ' phase [15], in agreement with the results of this study as demonstrated in the next section. Consequently, the greater density of Ta- and Ti-rich carbide phases in a polycrystalline alloy in comparison with its single-crystal version would be expected to reduce the lattice parameter of the γ' phase and in turn the extent of γ - γ' lattice mismatch influencing the growth kinetics of the γ' phase. As shown in the next section, the growth kinetics of the γ' phase in a single-crystal alloy was accelerated in comparison with its polycrystalline version, which could be related to the very small density of Ta- and Ti-rich carbides in the single-crystal alloy.

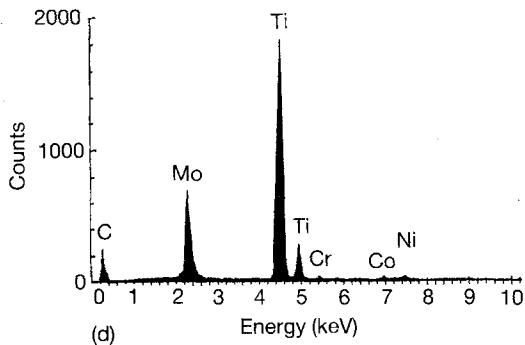
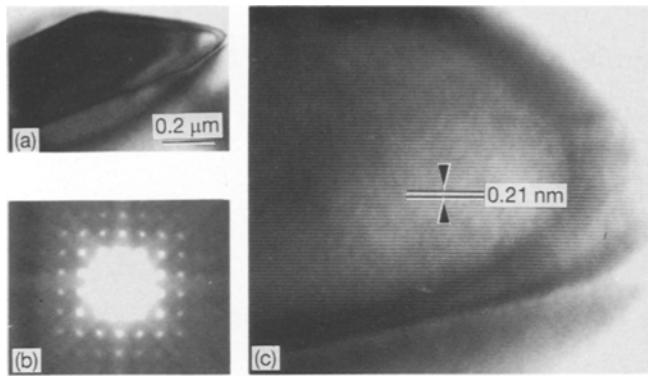


Figure 6 An example illustrating TEM-STEM analysis of an MC carbide particle in alloy RR 2000 (aged condition). (a) Bright-field TEM image of a carbide particle. (b) [001] convergent beam diffraction pattern derived from the particle in (a). (c) One-dimensional lattice fringe image of {200} planes of the carbide particle. (d) Energy-dispersive X-ray spectrum derived from the carbide particle in the STEM mode using an ultra-thin-window X-ray detector.

A similar effect could also be produced by an exact distribution of elements such as Mo and W partitioning to the matrix phase.

Frequently, dislocation tangles were observed at the carbide-matrix interface in the aged condition as illustrated in the example of Fig. 10a. It is possible that these dislocations had formed during cooling from the solution-annealing temperature to accommodate the strain resulting from differences in thermal expansion characteristics of the carbide and matrix. After exposure to higher temperatures, dislocations appeared to emanate from the carbide-matrix interface as shown in Fig. 10b. Such dislocations were suggested to significantly influence the extent of coherency between the γ' and γ phases during exposure to elevated temperatures [13]. However, the comparative behaviour of the alloys studied indicated that the above role of carbides was of little or no significance, as shown later.

3.3. Thermal stability of the γ' phase

In the case of alloys IN 100 and RR 2000, the lamellar γ' was enriched in Mo and for alloys MAR M 002 and SRR 99, it was found to be enriched in W as illustrated in the example of Fig. 11. In the case of alloys MAR M 002 and SRR 99, the lamellar γ' was also found to contain Ta as revealed by WDXS (Fig. 12). It is to be noted that at relatively small concentrations of Ta, it

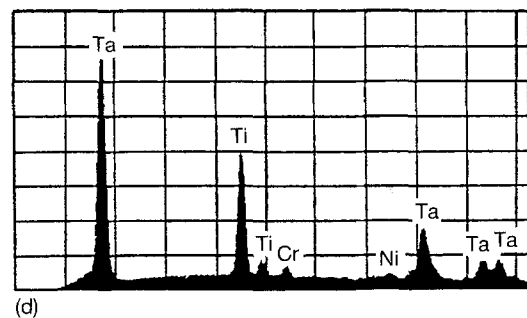
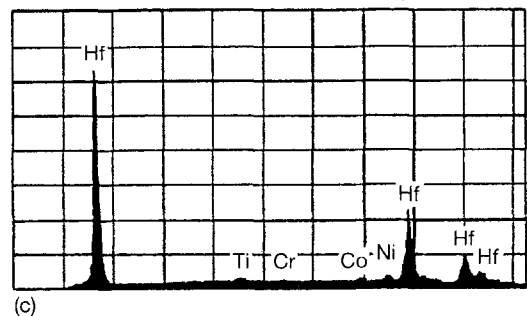
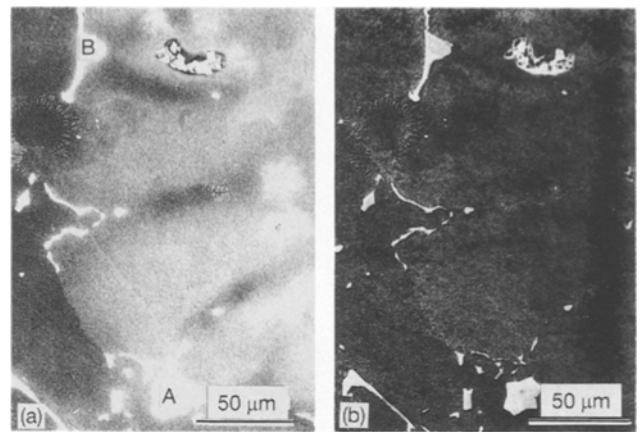


Figure 7 Conventional SEM-EDXS analysis illustrating the presence of two types of MC carbide in alloy MAR M 002 DS (aged condition). (a) Secondary electron SEM image (as-polished specimen). (b) Corresponding back-scattered electron composition image. (c) Energy-dispersive X-ray spectrum derived from the particle marked A in (a). (d) Energy-dispersive X-ray spectrum derived from the particle marked B in (a).

is not possible to distinguish between W and Ta by energy-dispersive spectroscopy because the energies of their strongest peaks ($W-M_{\alpha}$: 1.78 keV and $Ta-M_{\alpha}$: 1.71 keV) lie within the spectral resolution (about 0.15 keV). Similar to the case of carbides described earlier, the presence of Mo and W in the lamellar γ' could influence the lattice mismatch between the cuboidal γ' and the matrix.

An example illustrating TEM-STEM analysis of the cuboidal γ' in alloy MAR M 002 is given in Fig. 13. Since Co can substitute for Ni in the $L1_2$ superlattice, Ti for Al and Cr for both Ni and Al, the spectral data of Fig. 13 suggested that the composition of the cuboidal γ' was of the type $(Ni,Co,Cr)_3(Al,Ti,Ta,Cr)$. A similar result was obtained for alloy SRR 99. For both alloys, the Ti concentration in the spherical γ' was considerably smaller in comparison with the cuboidal

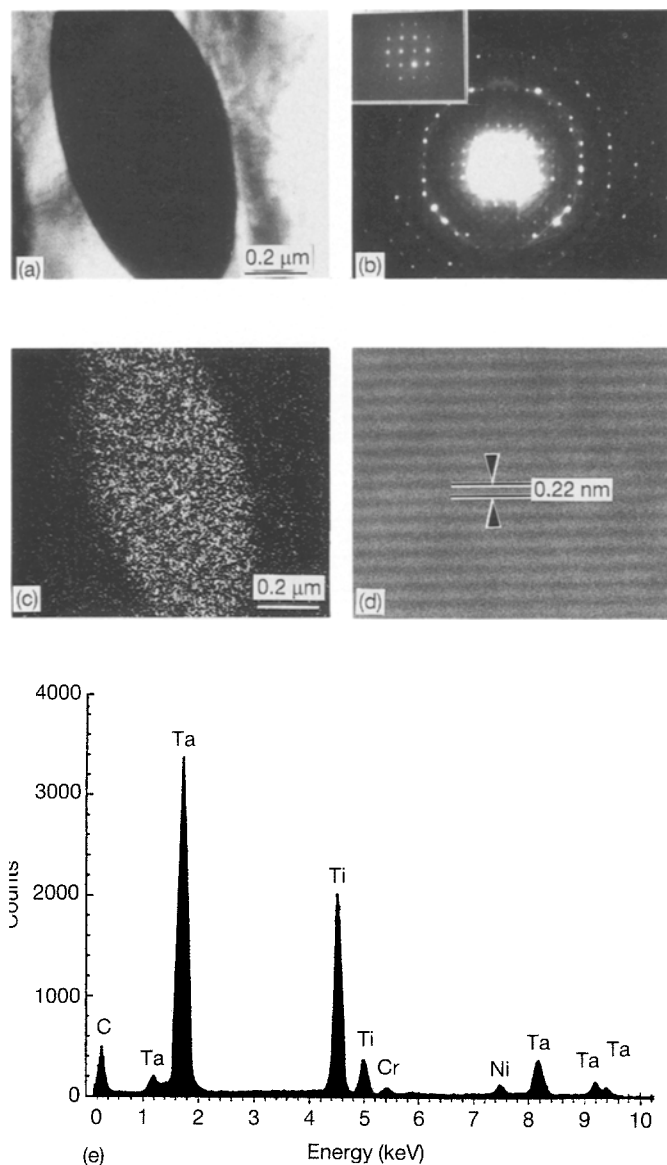


Figure 8 An example illustrating TEM-STEM analysis of (Ta,Ti)-rich carbide in alloy MAR M 002 DS (aged condition). (a) Bright-field STEM image of a carbide particle. (b) [001] convergent-beam diffraction pattern derived from the particle in (a); the zero-order Laue zone is shown in the inset. (c) X-ray mapping image of Ta. (d) One-dimensional lattice fringe image of {200} planes of the carbide particle. (e) Energy-dispersive X-ray spectrum derived from the carbide particle in the STEM mode using an ultra-thin-window X-ray detector.

γ' as shown in the example of Fig. 14. Evidently, most of the available Ti was consumed in forming the cuboidal γ' during ageing. The change of morphology from cuboidal to spherical as the Ti concentration was considerably reduced suggested that expansion of the $L1_2$ superlattice by the presence of Ti was rather significant, which is contrary to an earlier suggestion [23].

In the case of alloys IN 100 and RR 2000, the composition of the cuboidal γ' was found to be of the type $(\text{Ni},\text{Co},\text{Cr})_3(\text{Al},\text{Ti},\text{Cr})$. Also, the spherical γ' had a considerably lower Ti concentration.

Examples illustrating the effect of 900 h of exposure at 1000 and 1100 °C on the morphology of cuboidal γ' phase in alloys IN 100 and RR 2000 are shown in the

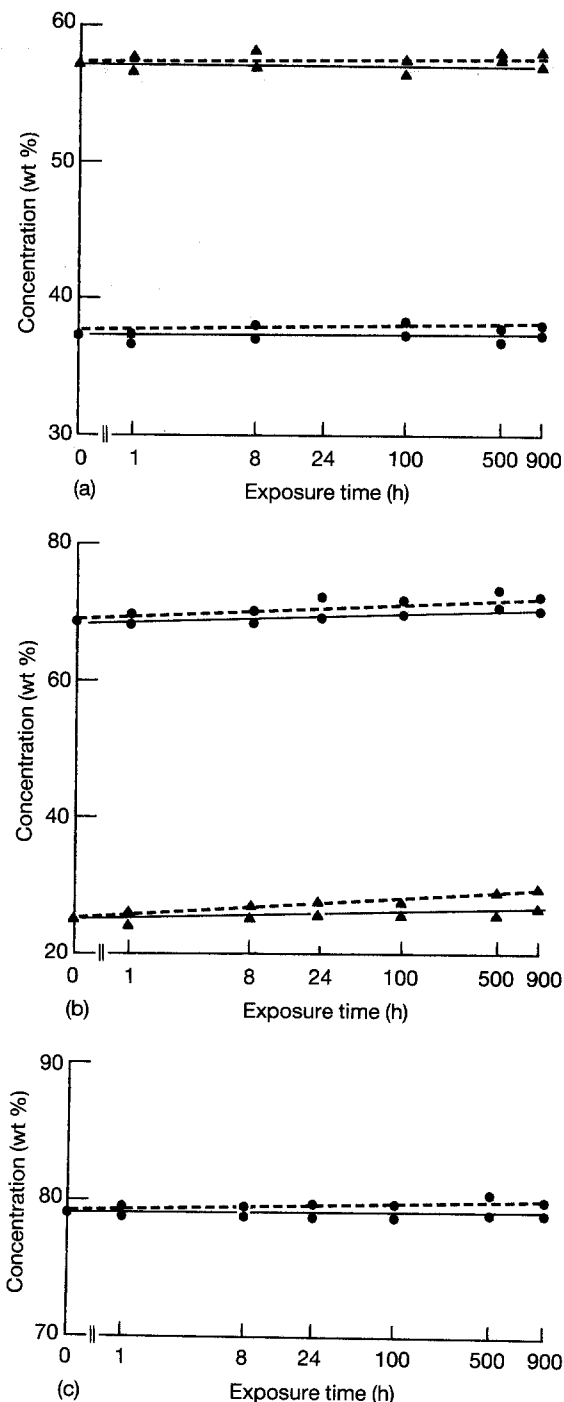


Figure 9 Effects of exposure time at (—) 1000 and (---) 1100 °C on the compositions of MC carbides in the alloys studied. (a) $(\text{Ti}_{0.8}\text{Mo}_{0.2})\text{C}$ carbide in alloys IN 100 and RR 2000: (●) Mo, (▲) Ti. (b) $(\text{Ta},\text{Ti})\text{C}$ carbide in alloys MAR M 002 DS and SRR 99: (●) Ta, (▲) Ti. (c) HfC carbide in alloy MAR M 002: (●) Hf.

secondary electron SEM images of Fig. 15. Relative to the aged condition, the γ' particles of both alloys were coarsened. For alloy IN 100, the coarsening was rather non-directional (Fig. 15a, c, e). In contrast, directional coarsening was considerably pronounced in alloy RR 2000. Directional coarsening was suggested to be accelerated by a larger γ' - γ lattice mismatch [15], which appeared to be consistent with the data of Table III. Based upon the overall compositions of the two alloys (Table I), particularly the Ti and Mo contents, a similar lattice mismatch would be expected.

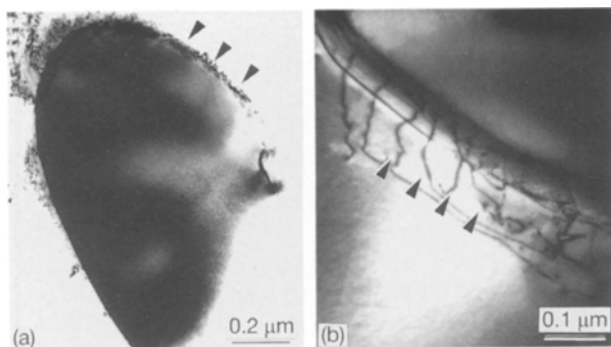


Figure 10 Examples of bright-field TEM images illustrating dislocation structures at carbide–matrix interfaces of alloy RR 2000 as indicated by the arrows: (a) aged condition, (b) exposed for 24 h at 1000 °C.

Evidently, however, redistribution of these elements in other phases (Mo in lamellar γ' reducing the lattice constant of the γ phase as well as Ti and Mo in MC carbide reducing the lattice constants of the γ' and γ phase, respectively) had a significant effect on the

lattice mismatch. A greater proportion of the Mo-rich lamellar γ' in alloy RR 2000 would be expected to increase the lattice mismatch due to depletion of the matrix phase in Mo. Also, the smaller density of the Ti-rich carbide in alloy RR 2000 could further contribute to increasing the lattice mismatch. Considerable loss of coherency, particularly in the case of alloy RR 2000, was evident from the observation of dislocation networks around the γ' particles as shown in Fig. 16a. Also, growth antiphase boundaries were frequently observed as illustrated in Fig. 16b and c. Contrary to earlier suggestions [13], the above results indicated that the role of carbide particles in providing dislocations contributing to loss of coherency was not significant, at least in the alloys studied.

Similar to the above case, the extent of directional coarsening in the single-crystal alloy SRR 99 was more pronounced in comparison with alloy MAR M 002 as summarized in Fig. 17a and b. For all alloys studied the spherical γ' was also coarsened, but the morphology remained unchanged as shown in the example of Fig. 17c.

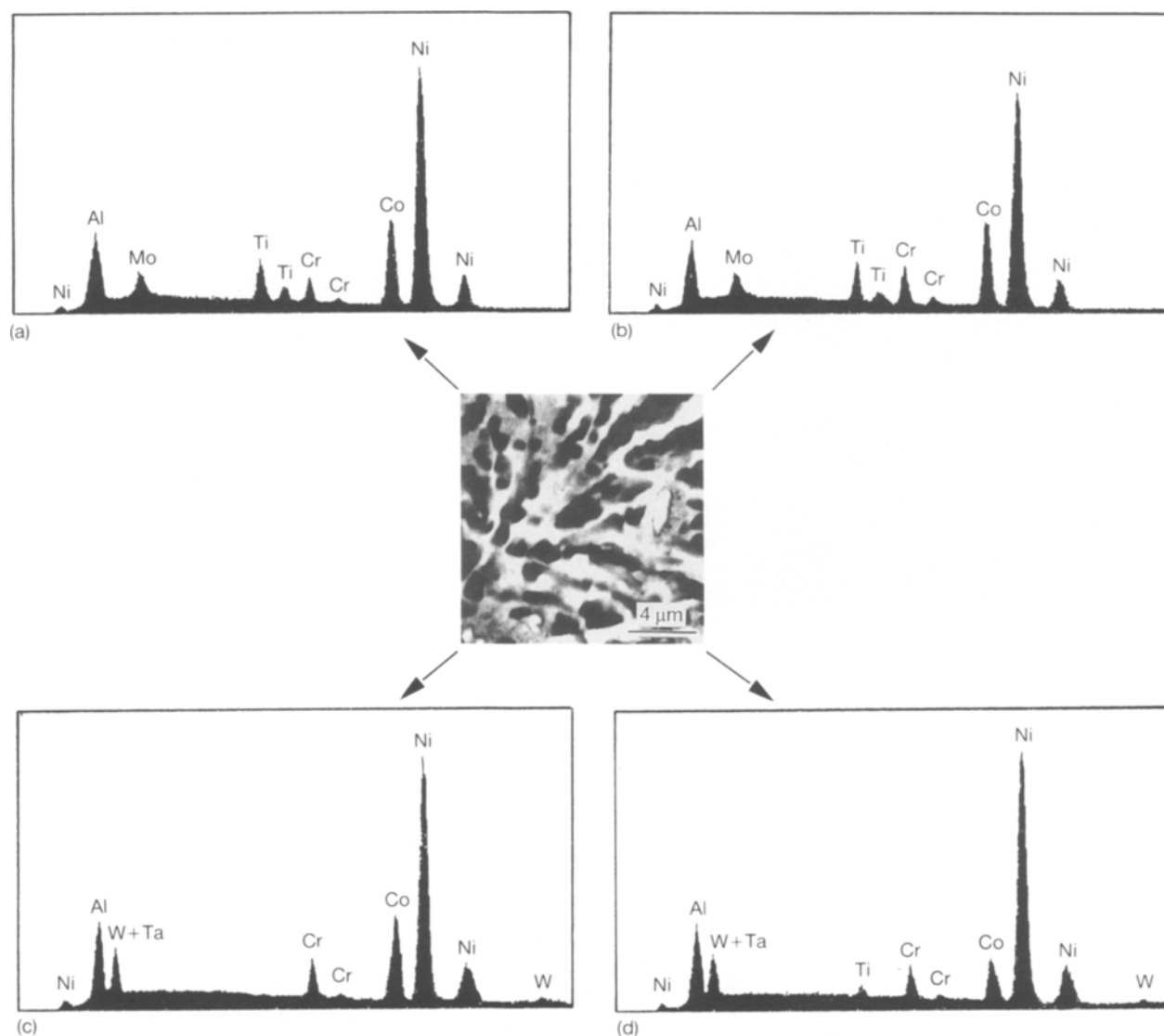


Figure 11 Conventional SEM–EDXS analysis of lamellar γ' phase in the alloys studied (aged condition), showing a representative secondary electron SEM image: (a) IN 100, (b) RR 2000, (c) MAR M 002 DS, (d) SRR 99.

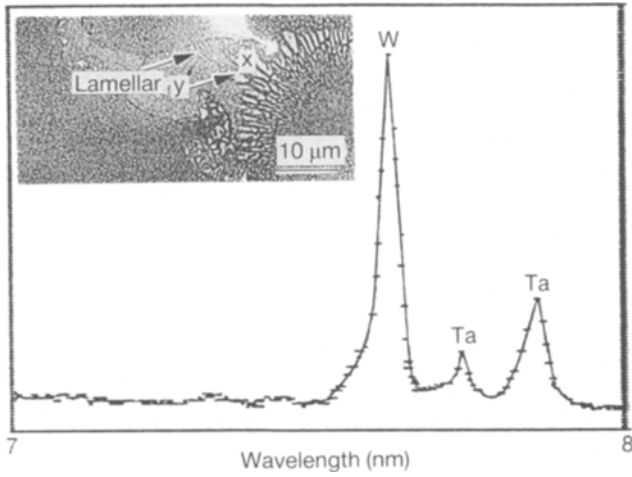


Figure 12 An example of WDXS analysis illustrating the enrichment of lamellar γ' phase in alloy MAR M 002 DS in both W and Ta; the spectrum is derived from the region marked x in the secondary electron SEM image of the inset.

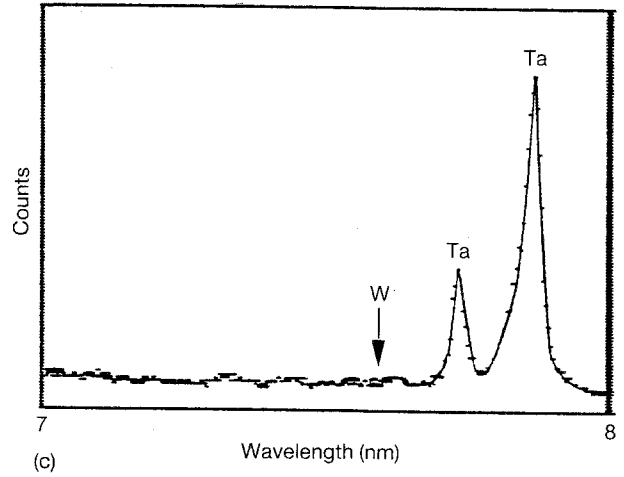


Figure 13 Analysis of cuboidal γ' phase in alloy MAR M 002 DS (aged condition). (a) Bright-field STEM image; a [001] micro-diffraction pattern corresponding to a particle such as that marked x is shown in the inset where characteristic reflections of the $L1_2$ superlattice are observed. (b) Energy-dispersive X-ray spectrum representative of the γ' phase (STEM analysis). (c) Wavelength-dispersive X-ray spectrum representative of the γ' phase and illustrating the absence of W; the position of the W peak is indicated by the arrow (electron microprobe analysis).

Fig. 18 illustrates the effect of exposure time at 1000 °C on the composition of cuboidal γ' phase in the alloys studied. Similar results were obtained for exposure at 1100 °C. For all exposure conditions, there was no significant change in the γ' composition. Both the Al and Ti concentrations decreased only slightly with

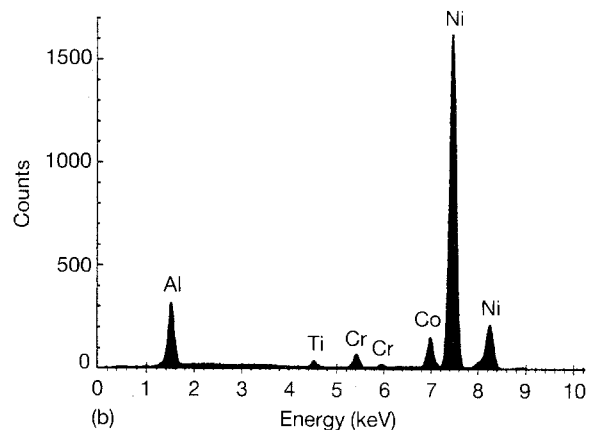
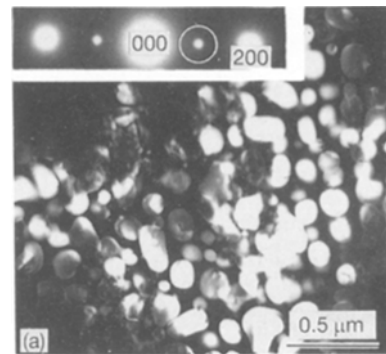
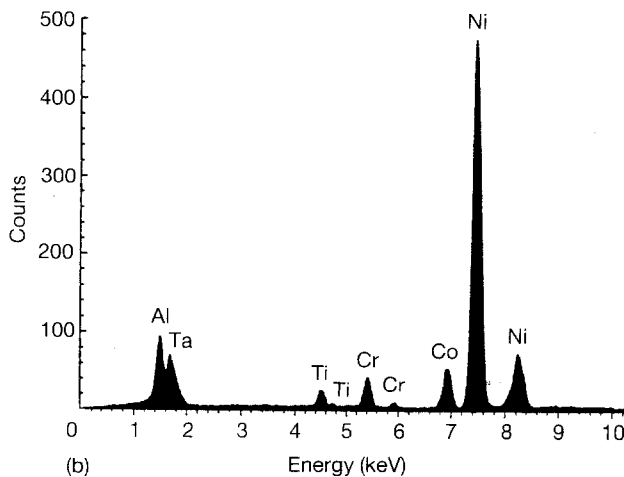
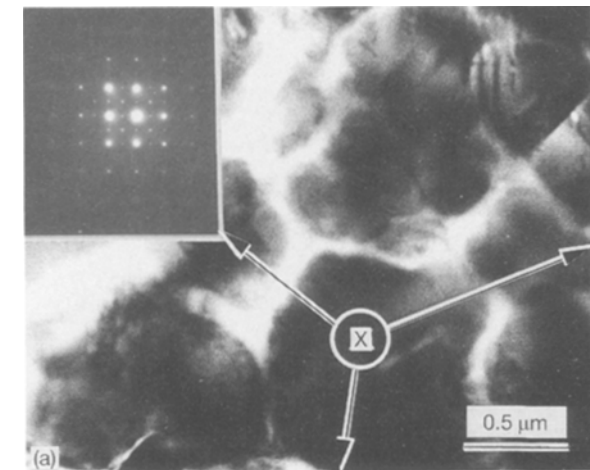


Figure 14 Analysis of cooling γ' phase in alloy MAR M 002 DS (aged condition). (a) Dark-field TEM image formed with the encircled (100) superlattice reflection in the selected-area diffraction pattern of the inset. (b) Energy-dispersive X-ray spectrum representative of the γ' phase (STEM analysis).

exposure time. There was also a slight increase in the Ni concentration. However, the Ta concentration (alloys MAR M 002 and SRR 99) remained unchanged. Similar results were reported for other alloys [14].

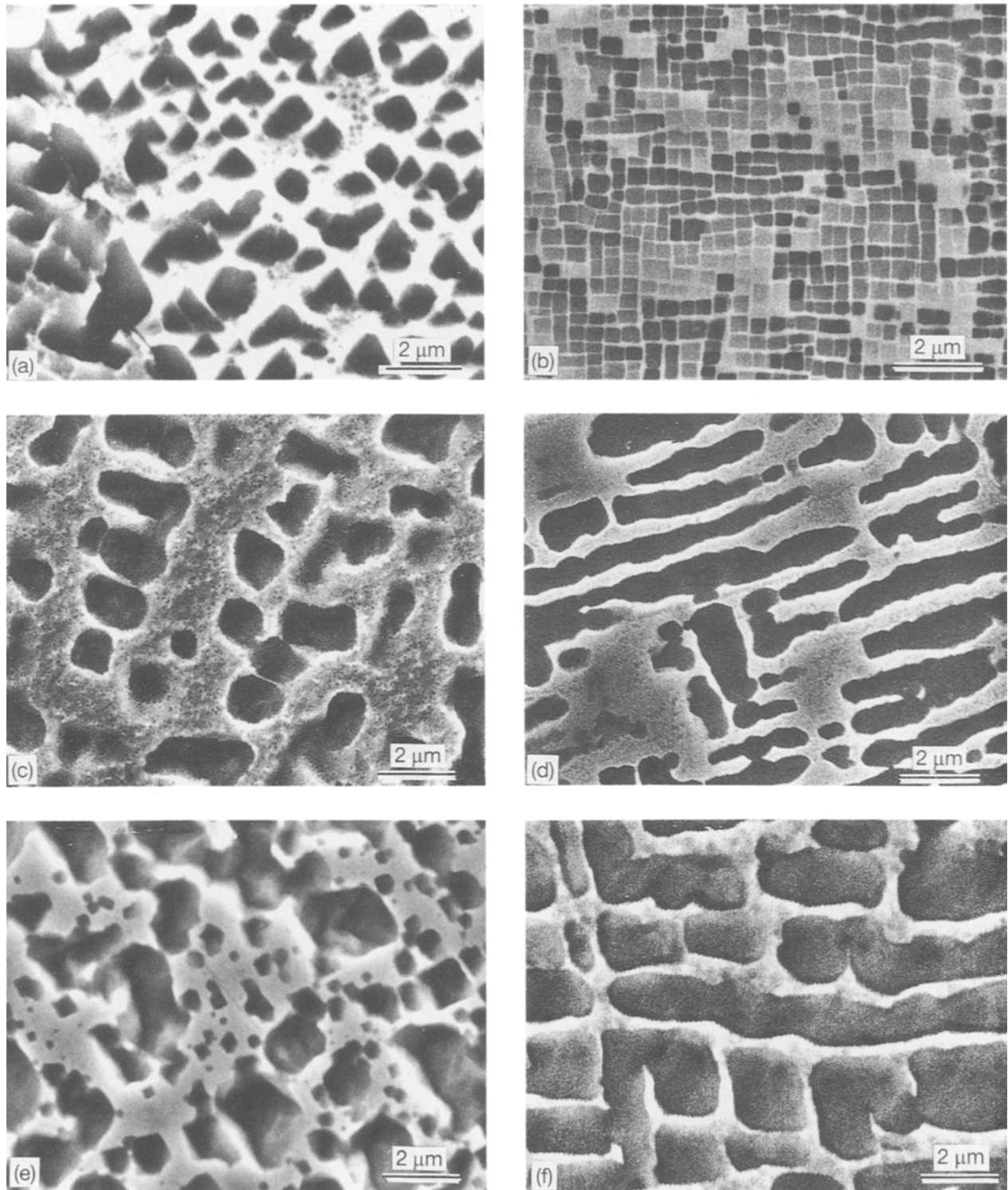


Figure 15 Secondary electron SEM images illustrating the effect of 900 h of exposure at 1000 and 1100 °C on the morphology of cuboidal γ' phase in alloys (a, c, e) IN 100 and (b, d, f) RR 2000: (a, b) aged; (c, d) 1000 °C, (e, f) 1100 °C.

Another important effect of exposure at 1000 and 1100 °C was the decrease in volume fraction of cuboidal γ' phase as summarized in Fig. 19. As can be seen, the decrease in volume fraction was almost identical for alloys IN 100 and RR 2000. Also, alloys MAR M 002 and SRR 99 followed a similar behavior; however, for all exposure conditions they maintained a larger volume fraction in comparison with alloys IN 100 and RR 2000. It is to be noted that the γ' solvus temperature of alloys MAR M 002 and SRR 99 is about 100 °C higher in comparison with alloys IN 100 and

RR 2000, thus explaining the above observation. Such a difference in behaviour could be related to the presence of W in alloys MAR M 002 and SRR 99, leading to a higher γ' solvus temperature [15].

3.4. Thermal stability of the γ phase

In contrast with the case of γ' phase described above, the composition of the matrix solid solution (γ phase) was observed to significantly change with exposure time at 1000 and 1100 °C. For all alloys, both the Al

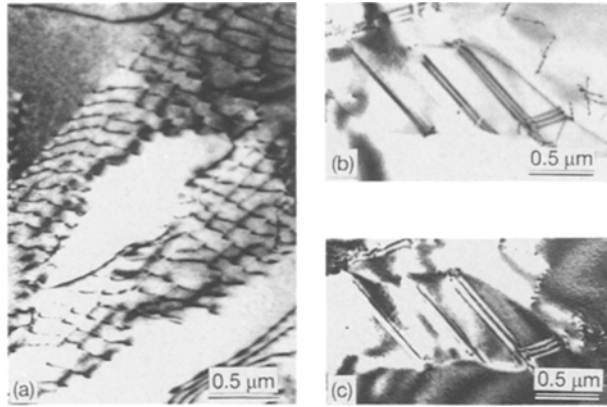


Figure 16 Examples of TEM images illustrating the effect of 900 h of exposure at 1000 °C on the structural features of cuboidal γ' phase in alloy RR 2000. (a) Bright-field TEM image illustrating a dislocation network at the γ - γ' interface. (b) Bright-field TEM image illustrating fringe contrast in a γ' particle due to the presence of antiphase boundaries. (c) Corresponding dark-field image.

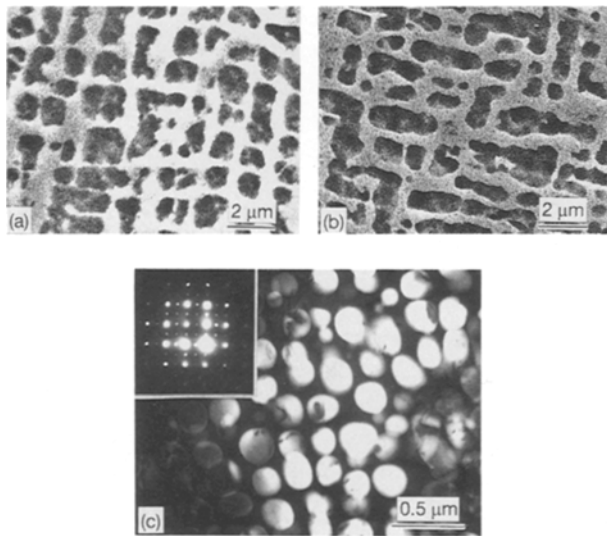


Figure 17 Examples illustrating the effect of 900 h of exposure at 1000 °C on the morphology of cuboidal and spherical γ' phases in alloys MAR M 002 DS and SRR 99. (a) Secondary electron SEM image illustrating the cuboidal γ' phase in MAR M 002 DS. (b) Secondary electron SEM image illustrating the cuboidal γ' phase in SRR 99. (c) Representative dark-field TEM image of spherical γ' phase; a corresponding [001] microdiffraction pattern is shown in the inset.

and Ti concentrations increased by about 20% after 900 h of exposure at 1000 °C and about 30% after 1000 h of exposure at 1100 °C. Also, concentrations of Cr and Co were decreased by about 15–20% and 25–30% after 900 h of exposure at 1000 and 1100 °C, respectively. However, within the relative accuracy of EDXS (1–5%), the concentrations of Mo (alloys IN 100 and RR 2000) and W (alloys MAR M 002 and SRR 99) remained essentially unchanged. Such changes in composition could result from the dissolution of γ' phase and its relatively constant composition.

Another effect of thermal exposure was the precipitation of the sigma phase. Precipitates of sigma phase identified by electron diffraction were observed in all alloys studied after 100 h of exposure at 1000 °C. As

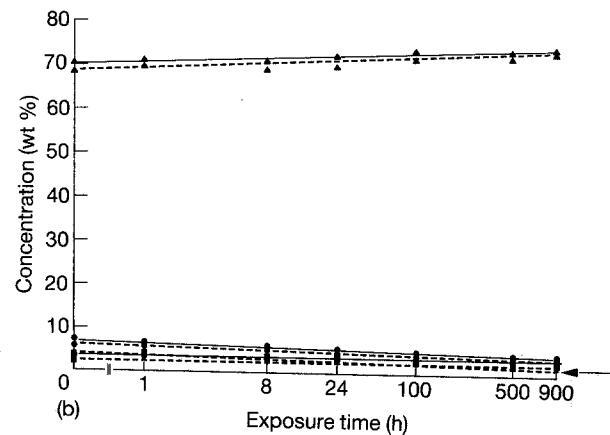
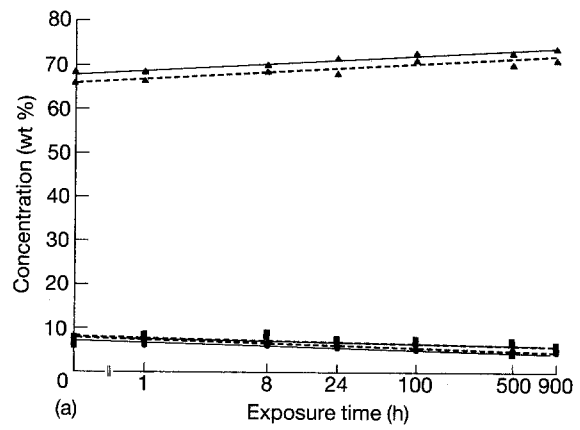


Figure 18 Effect of exposure time at 1000 °C on the concentrations of various elements in the cuboidal γ' phase of the alloys studied: (a) (---) IN 100 and (—) RR 2000. (b) (—) MAR M 002 DS and (---) SRR 99. (●) Al, (■) Ti, (▲) Ni, (◆) Ta.

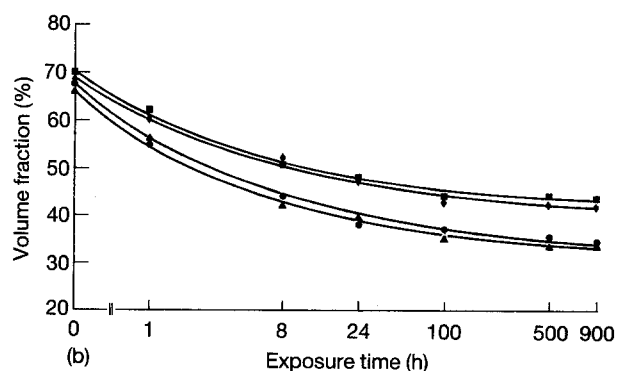
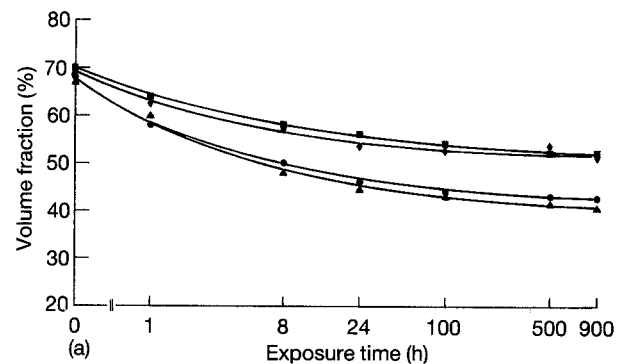


Figure 19 Effect of exposure time at (a) 1000 and (b) 1100 °C on the volume fraction of cuboidal γ' phase in the alloys studied: (●) IN 100, (▲) RR 2000, (■) MAR M 002 DS, (◆) SRR 99.

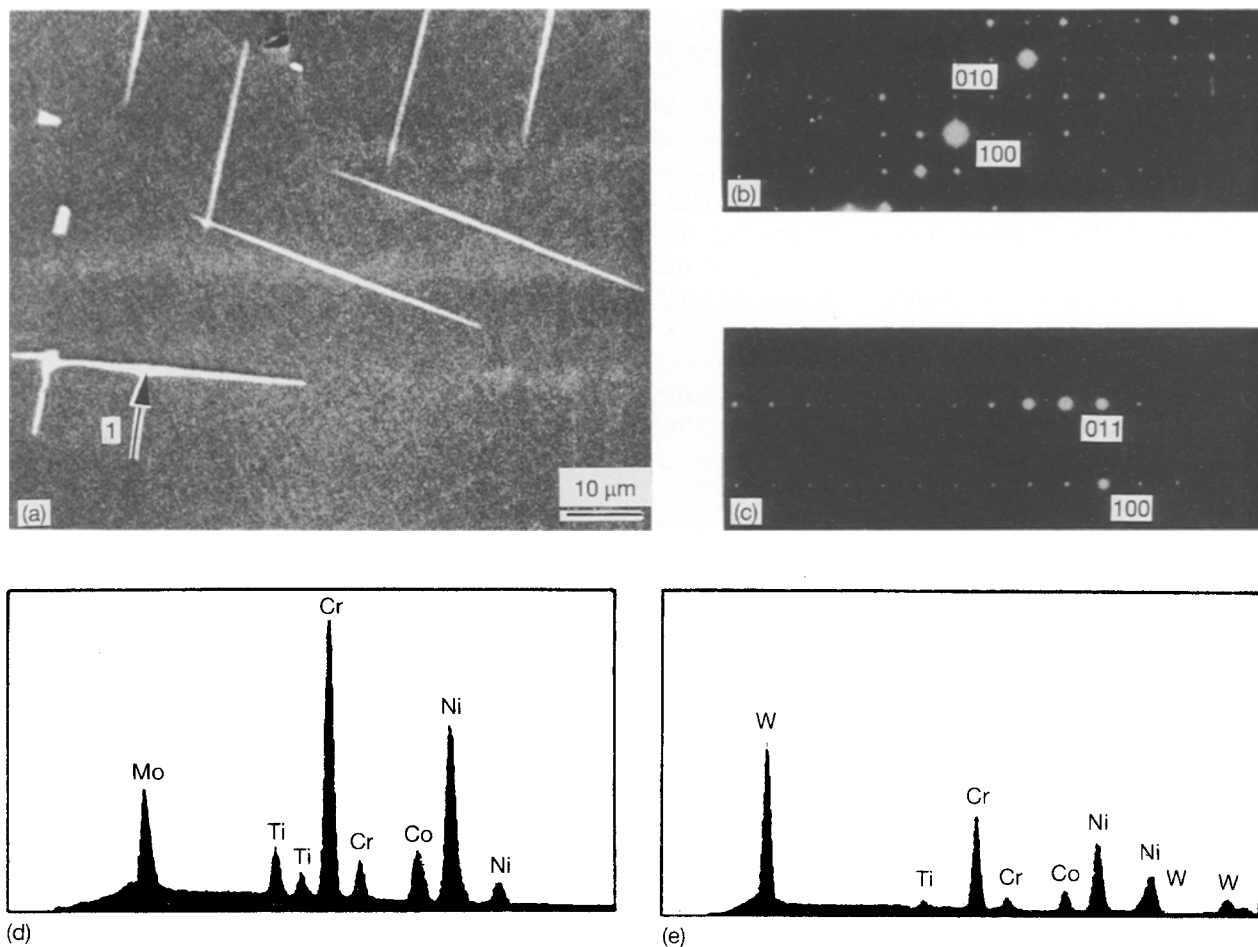


Figure 20 Identification of sigma-phase precipitates in the alloys studied after 500 h or exposure at 1000 °C. (a) Example of a secondary electron SEM image showing platelets of sigma phase (marked 1) in alloy SRR 99, (as-polished specimen). (b) Representative [001] microdiffraction pattern of the sigma phase. (c) Representative [011] microdiffraction pattern of the sigma phase. (d) Representative energy-dispersive X-ray spectrum of the (Ni + Co)-Cr-Mo sigma phase in alloy IN 100 and RR 2000. (e) Representative energy-dispersive X-ray spectrum of the (Ni + Co)-Cr-W sigma phase in alloys MAR M 002 and SRR 99.

illustrated in the example of Fig. 20a, the sigma phase assumed a platelet-type morphology. Characteristic microdiffraction patterns of the tetragonal sigma phase in [001] and [011] orientations are shown in Fig. 20b and c, respectively. In the case of alloys IN 100 and RR 2000, the composition of the sigma phase was essentially of the type (Ni + Co)-Cr-Mo as shown in the representative energy-dispersive X-ray spectrum of Fig. 20d. It is known that the sigma phase exists in Ni-Cr-Mo over a wide range of composition and that Co can substitute for Ni [35]. For alloys MAR M 002 and SRR 99, the sigma phase composition was of the type (Ni + Co)-Cr-W as shown in the example of Fig. 20e. Also, this type of sigma phase is known to exist over a wide range of composition in the Ni-Cr-W system [35].

As the exposure temperature was raised from 1000 to 1100 °C, precipitates of sigma phase were observed only in alloys MAR M 002 and SRR 99. This behaviour could be due to the greater thermal stability of the Ni-Cr-W sigma phase in comparison with the Ni-Cr-Mo sigma phase [35].

3.5. Effect of thermal exposure on microhardness

Fig. 21 summarizes the effect of exposure time at 1000 and 1100 °C on the room-temperature microhardness

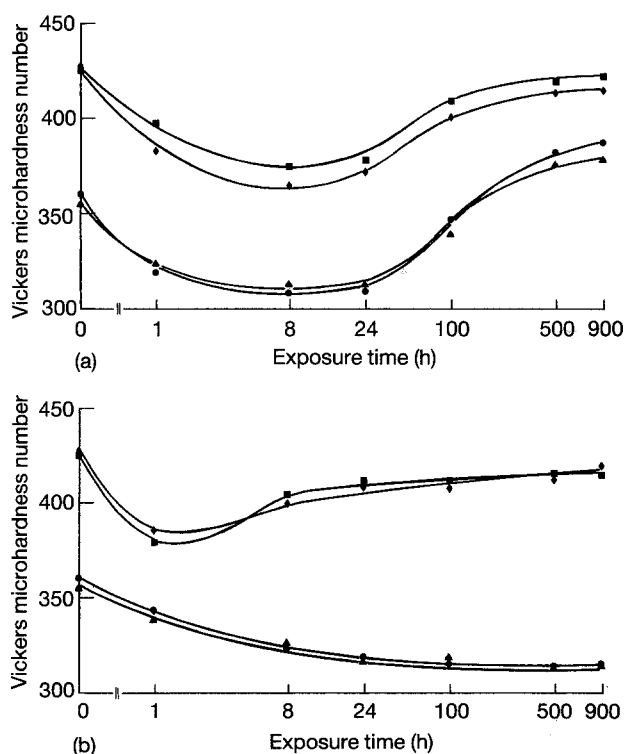


Figure 21 Effect of exposure time at (a) 1000 °C and (b) 1100 °C on the room-temperature microhardness of the alloys studied: (●) IN 100, (▲) RR 2000, (■) MAR M 002 DS, (◆) SRR 99.

of the alloys studied. During the initial stages of exposure at 1000 °C (Fig. 21a), the microhardness of each alloy was observed to decrease relative to the aged condition. With continued exposure, however, the microhardness was increased. Based upon the results presented earlier, the initial decrease in microhardness could be explained in terms of the partial dissolution of the γ' phase. Subsequent precipitation of the extremely hard sigma phase could explain the observed increase in microhardness during the later stages of exposure.

A similar behaviour to that described above was observed for alloys MAR M 002 and SRR 99 as the exposure temperature was raised to 1100 °C (Fig. 21b). In contrast, no hardening effect was experienced by alloys IN 100 and RR 2000. This behaviour could be explained in terms of the instability of sigma phase in these alloys at 1100 °C.

4. Conclusions

In the aged condition of selected Ni-based superalloys, the nature of the interface separating the strengthening γ' phase (cuboidal morphology) from the surrounding matrix was found to vary on an atomic scale from coherent to partially coherent. Both the alloy composition and distribution of key elements in coarse lamellar γ' and carbide phases were found to influence the lattice mismatch. Directional growth of the strengthening γ' phase upon exposure to higher temperatures was accelerated by a large initial lattice mismatch leading to a considerable loss of coherency. Partial dissolution of the γ' phase occurred at an essentially constant composition, leading to a marked change in matrix composition. Associated with this dissolution during the early stages of exposure was a decrease in room-temperature microhardness; however, a hardening effect was experienced during the later stages of the exposure due to precipitation of sigma phase.

Acknowledgements

It is a pleasure to acknowledge the financial support of Rolls-Royce plc who also provided the materials used in this study. The support of the Research Institute of King Fahd University of Petroleum and Minerals, where this study was carried out, is also greatly appreciated.

References

1. N. S. STOLOFF and C. T. SIMS, in "Superalloys II", edited by C. T. Sims, N. S. Stoloff and W. C. Hagel (Wiley, New York, 1987) p. 519.
2. C. T. SIMS, *Advanced Mater. Process.* **139** (6) (1991) 32.
3. W. J. MOLLOY, *ibid.* **138** (4) (1990) 23.
4. C. H. WHITE, P. M. WILLIAMS and M. MORLEY, *ibid.* **137** (4) (1990) 53.
5. G. K. BOUSE and J. R. MIHALISIN, in "Superalloys, Supercomposites and Superceramics", edited by J. K. Tien and T. Caulfield (Academic, New York, 1989) p. 99.
6. D. DRIVER, "Materials at their Limit" (Institute of Metals, London, 1986) p. 519.
7. D. N. DUHL, in "Superalloys II", edited by C. T. Sims, N. S. Stoloff and W. C. Hagel (Wiley, New York, 1987) p. 189.
8. *Idem*, in "Superalloys, Supercomposites and Superceramics", edited by J. K. Tien and T. Caulfield (Academic, New York, 1989) p. 149.
9. B. H. KEAR and D. P. POPE, *ibid.* p. 545.
10. B. H. KEAR and E. R. THOMPSON, *Science* **208** (1980) 847.
11. N. S. STOLOFF, *Int. Met. Rev.* **34** (4) (1989) 153.
12. D. P. POPE and S. S. EZZ, *ibid.* **29** (3) (1984) 136.
13. A. K. SINGH, N. LOUAT and K. SADANADA, *Met. Trans.* **19A** (1988) 2965.
14. G. M. JANOWSKI, B. S. HARWON and B. J. PLETKA, *ibid.* **18A** (1987) 1341.
15. V. NATHAL and E. J. EBERT, *ibid.* **16A** (1985) 1849.
16. H. E. COLLINS, *ibid.* **5** (1974) 189.
17. E. H. Van Der MOLEN, J. M. OBLAK and O. H. KRIEGE, *ibid.* **2** (1971) 1627.
18. H. E. COLLINS, *Trans. ASM* **62** (1969) 82.
19. H. E. COLLINS and R. J. QUIGG, *ibid.* **61** (1968) 139.
20. T. LINK and M. FELLER-KNIEPMEIER, *ibid.* **23A** (1992) 99.
21. J. H. ZHANG, Z. Q. HU, Y. B. XU and Z. G. WANG, *ibid.* **23A** (1992) 1253.
22. E. W. ROSS and C. T. SIMS, in "Superalloys II", edited by C. T. Sims, N. S. Stoloff and W. C. Hagel (Wiley, New York, 1987) p. 97.
23. S. T. WLODEK, *Trans. ASM* **57** (1964) 110.
24. C. HAMMOND and J. NUTTING, *Met. Sci. J.* **11** (1977) 474.
25. R. L. DRESHFIELD, *J. Met.* **39** (7) (1987) 16.
26. E. E. UNDERWOOD, in "Metallography, Structure and Phase Diagrams", Metals Handbook, Vol. 8, 8th Edn (ASM, Metals Park, Ohio, 1973) p. 37.
27. S. FLOREEN, in "Superalloys II", edited by C. T. Sims, N. S. Stoloff and W. C. Hagel (Wiley, New York, 1987) p. 241.
28. R. G. DAVIES and T. L. JOHNSTON, in "Ordered Alloys: Structural Applications and Physical Metallurgy", edited by B. H. Kear, C. T. Sims, N. S. Stoloff and J. H. Westbrook (Claitor's Publishing Division, Baton Rouge, Louisiana, 1970) p. 447.
29. B. H. KEAR, in "Order-Disorder Transformation in Alloys", edited by H. Warlimont (Springer, New York, 1974) p. 440.
30. B. R. CLARK and F. B. PICKERING, *J. Iron Steel Inst.* **205** (1967) 70.
31. B. A. PARKER and D. R. F. WEST, *J. Austral. Inst. Metals* **14** (1969) 102.
32. J. HESLOP, *Cobalt* **24** (1964) 1.
33. C. H. WHITE, in "The Nimonic Alloys", edited by W. Beteridge and J. Heslop (Crane, Russak Co., New York, 1974) p. 63.1.
34. P. HIRSCH, A. HOWIE, R. B. NICHOLSON, D. W. PASHLEY and M. J. WHELAN, "Electron Microscopy of Thin Crystals" (Krieger, Huntington, New York, 1977) p. 317.
35. G. WALLWORK and J. CROLL, in "Review of High Temperature Materials", Vol. III, No. 2, edited by J. B. Newkirk (Freund, Tel Aviv, Israel, 1976) p. 89.

Received 7 January
and accepted 6 October 1993